

High-Resolution Population Grid in the CONUS Using Microsoft Building Footprints: A Feasibility Study

Xiao Huang

Department of Geography
University of South Carolina
Columbia, SC, USA
xh1@email.sc.edu

Cuizhen Wang

Department of Geography
University of South Carolina
Columbia, SC, USA
cwang@mailbox.sc.edu

Zhenlong Li

Department of Geography
University of South Carolina
Columbia, SC, USA
zhenlong@mailbox.sc.edu

ABSTRACT

Better knowledge of where people live is of great importance for a wide range of studies, including disaster responses, public health, resource management, and urban planning. Given the increasing demand for population grid with improved quality, this study explores the feasibility of generating high-resolution (100m) population grids in the Conterminous U.S. (CONUS) using a total of 125 million building footprints recently released by Microsoft. Those building footprints were used to disaggregate census tract population of the latest ACS 5-year estimates (2013-2017). Land use dataset from the OpenStreetMap (OSM) was applied to trim raw buildings footprints by removing those that are not likely residential. Weighting scenarios were designed, with which a dasymetric model was applied to disaggregate the ACS census tract estimates into a 100m population grid product. The results suggest that building footprints as a weighting layer, particularly footprint size after trimming, outperforms other commonly used weighting layers and is able to capture the great heterogeneity of population distribution at the micro-level. This study provides valuable experience in developing high-resolution population grid products that can benefit a wide range of studies in need of spatially explicit population data.

CCS CONCEPTS

- Information systems → Geographic information systems;
- Applied computing → Cartography;

KEYWORDS

Population grid, Microsoft building footprints, dasymetric mapping, population disaggregation

Permission to make digital or hard copies of all or part of this work for personal or classroom use is granted without fee provided that copies are not made or distributed for profit or commercial advantage and that copies bear this notice and the full citation on the first page. Copyrights for components of this work owned by others than the author(s) must be honored. Abstracting with credit is permitted. To copy otherwise, or republish, to post on servers or to redistribute to lists, requires prior specific permission and/or a fee. Request permissions from Permissions@acm.org.

GeoHumanities'19, November 5, 2019, Chicago, IL, USA

© 2019 Copyright is held by the owner/author(s). Publication rights licensed to ACM.

ACM ISBN 978-1-4503-6960-2/19/11...\$15.00

<https://doi.org/10.1145/3356991.3365469>

ACM Reference format:

Xiao Huang, Cuizhen Wang, and Zhenlong Li. 2019. High-Resolution Population Grid in the CONUS Using Microsoft Building Footprints: A Feasibility Study. In *GeoHumanities'19: 3rd ACM SIGSPATIAL Workshop on Geospatial Humanities, November 5–8, 2019, Chicago, Illinois, USA*. ACM, New York, NY, USA, 9 pages. <https://doi.org/10.1145/3356991.3365469>

1 INTRODUCTION

Knowing where people are living at the local level is essential for a broad range of studies, including disaster responses and assessments [1], humanitarian relief operations [2], public health [3], resource management [4] and urban planning [5,6]. Population, however, as a fundamental agent in the urban and suburban ecosystem, is distributed with great heterogeneity [7]. Therefore, great uncertainty might be induced when a uniform distribution has to be assumed due to the lack of high spatial resolution population data [8].

In the U.S., official population data, the American Community Survey (ACS), for example, is commonly reported at different geographical levels. Despite the variety of levels, from the level of state to the level of block group, it often fails to satisfy the demand because 1) population does not follow uniform distribution within areal units given its intrinsic heterogeneity, therefore aggregate population data do not necessarily represent real population distribution [8]; 2) “population at risk”, the estimation of population in an area declared as under risk, does not usually follow existing census boundaries, causing great difficulty particularly when disastrous boundary is highly incompatible with census boundary [9]. 3) population in administrative boundaries is often spatially incomputable with other environmental data (e.g., gridded temperature) and temporally incompatible as a result of the everchanging boundary of the spatial unit [7]. 4) the discontinuity caused by the artifact of underlying arbitrary statutory boundaries potentially increases the uncertainty caused by the Modified Areal Unit Problem (MAUP) [10]. To overcome the limitations of such aggregate population data and to describe spatial variations within predefined boundaries, studies have targeted on generating spatially continuous population representation, i.e., population grid.

This study aims to explore the potential of building footprints in generating population grids at continental scale. The CONUS that covers 48 states was selected as the study area. Under the assumption that buildings act as a proxy for where people live, newly released Microsoft building footprints were used to disaggregate census tract population from the ACS 5-year estimates (2013-2017) into a 3 arc-second population grid (around 100m at the Equator). The disaggregation process was then evaluated using the population in each block group, a smaller geographical unit, as ground truth. Three weighting scenarios using building footprint statistics were explored: 1) cell with building footprint total counts; 2) cells with building footprint total size; and 3) cell with total count and total size combined (count*size). The effectiveness of building footprints in disaggregating population was further tested against commonly used weight layers, including the uniform layer, the light intensity layer, the land cover layer, and the impervious surface layer. The result of this study provides valuable experience in creating population grid products and could benefit a wide range of studies that require accurate high-resolution population grids.

2 ISSUES AND SOLUTIONS

Existing large-scale population grid products include History Database of the Global Environment (HYDE) Population Grids [11,12], Gridded Population of the World (GPW)-Version 4 (latest version) [13], Global Rural Urban Mapping Project (GRUMP) [14], Global Human Settlement– Population (GHS-POP) [15], LandScan Global Population database [16], World Population Estimate (WPE) [17], WorldPop [18] and Gridded Population Mapping [19]. Widely used population grid products like GPW, GRUMP, GHS-POP, and LandScan, are with a resolution of 30 arc-seconds (approximately 1km at the equator). Population grid products with sub-km resolution started to emerge in recent years, most notably the WorldPop and WPE, thanks to the growing need for a higher level of geographic precision in population distribution. However, the intrinsic limitations of those products above lie in the limited capability of weighting layers in summarizing population distribution at micro-level, leading to significant accuracy decay in rural areas where the population is rather sparse [20].

With the development of high-resolution satellite imagery and the surge in research on computer vision, detection of an individual building at large scale becomes possible [21,22]. Building footprints are assumed to outperform commonly used variables in population disaggregation for the following reasons: 1) people live in the buildings. Therefore the distribution of building footprints can well summarize population distribution patterns of both rural and urban areas; 2) building count (or building size) is a more sensitive and more direct linkage to population distribution than other often-used variables such as light intensity and distance to roads, which suffer from great uncertainty in estimating population distribution; 3) building footprints, often derived from sub-meter images, represent a weighting layer with much higher resolution compared to other commonly used weighting layers. A few studies have already explored the potential of building footprints in disaggregating census population down to the sub-km level, and

their results are rather promising [20,23]. Murdock et al. [23], for example, redistributed the population in England and Wales to residential buildings using a dasymetric mapping approach. In June 2018, the Bing Maps team from Microsoft released more than 125 million computer-generated building footprints covering the entire U.S. In comparison, OpenStreetMap (OSM), a popular crowdsourced platform, currently only contains a total of 30 million (OSM data downloaded on March 1st, 2019). At the time of writing, this Microsoft building footprint product is believed to be the newest and the most comprehensive building footprints for the entire U.S. Thus, its potential in generating large-scale population grid with high-resolution deserves further exploration.

3 DATASETS AND PREPROCESSING

3.1 Microsoft Building Footprints

Microsoft building footprint dataset was released in July 2018. Relying on the Microsoft Cognitive Toolkit (CNTK), the Bing Maps team has released more than 125 million computer-generated building footprints extracted from Bing imagery with a coverage of 50 U.S. states. Trained by 5 million labeled images, the resulted output reaches 99.3% as precision and 93.5% as recall [24]. The building footprints used in this study cover the entire CONUS with 48 states (D.C included). The total number of building footprints in CONUS is 124,828,547, and they were further projected using U.S. Albers equal-area conic projection to obtain their proper sizes. Given that Bing imagery is a composite of multiple sources, the date of extracted building footprints varies. The released dataset only contains the pure geometry of extracted building footprints, meaning that information such as building height and building type are not included. Despite the aforementioned limitations, this dataset (at the time of writing) is still the newest and most comprehensive open-source building footprints available for the entire U.S. We observed a wide existence of small footprints that are not likely habitable buildings (e.g., garages and trailers). To remove those small polygons, we set the minimum footprint size to be 50 m². Extra-large footprints were removed by a maximum threshold of 5,000 m².

3.2 OSM Land Use

OSM is a collaborative project that consists of a very detailed, dynamically updated spatial database of mapped features in the world from millions of voluntary contributors within an open-source environment [25]. Given its merit of massive and voluntary public participation, it provides a more detailed representation of land use than satellite-based classification. OSM data covering the entire CONUS was downloaded on March 1st from GEOFABRIK (<https://www.geofabrik.de/geofabrik/>), where OSM data are updated on a daily basis. As of March 1st, OSM land use in CONUS contains a total of 1,714,072 polygons with 19 unique land use classes. OSM land use polygons in this study were used to trim raw Microsoft building footprint dataset by removing non-residential building footprints. Due to the incomprehensiveness of the residential type in the OSM dataset, we didn't select buildings with

residential type directly. Instead, building footprints were removed if they were within OSM polygons of non-residential types, including allotments, commercial, farm, forest, grass, park, recreation ground, retail, vineyard, health, industrial, meadow, military, natural reserve, orchard, quarry, scrub, and cemetery. The remaining building footprints have high chances of being residential.

3.3 Population Dataset

The population dataset used in this study was derived from the ACS 5-year estimate (2013-2017) by the U.S. Census Bureau. The 2013-2017 ACS population data has been collected through a 60-month period from Jan 1st, 2013 to Dec 31st, 2017. The CONUS is composed of 72,538 census tracts and 266,330 block groups (smallest geographic area provided by the ACS 5-year estimates). Different weighting scenarios were tested to disaggregate the population in census tracts to 100m population grid using a dasymetric mapping technique. The derived population grid was then reaggregated to block group, a smaller geographic unit than census tract, for validation purposes.

3.4 Nighttime imagery, Land cover and Impervious surface

Numerous studies have reported a high correlation between nighttime light intensity and population density, making it a popular weighting layer for population disaggregation [26,27]. The nighttime light data used in this study was derived from the Suomi National Polar-orbiting Partnership Visible Infrared Imaging Radiometer Suite (VIIRS). The VIIRS nighttime data for 2017 were obtained from the NOAA National Centers for Environmental Information (NCEI). These data include monthly average radiance composite imagery (from Jan 2017 to Dec 2017) generated using the nighttime data of the VIIRS Day/Night Band (DNB) in the Suomi NPP satellite. The spatial resolution is 15 arc-second (742 m), and the Digital Number (DN) unit is $nW \cdot cm^{-2} \cdot sr^{-1}$ [28]. Before averaging to monthly products, the DNB data have been filtered to exclude data impacted by stray light, lightning, lunar illumination, and cloud cover [29]. The 12 monthly products from 2017 were further processed to derive a mean annual composite. The annual composite was then resampled to 100m to match the population grid size.

The effectiveness of applying land cover and impervious surface to perform population disaggregation has been confirmed by many, as they largely limit population distribution to built-up human environments, thus increasing the disaggregation accuracy [30]. The land cover and impervious surface data in the CONUS were produced by the National Land Cover Database (NLCD) and were downloaded from Multi-Resolution Land Characteristics Consortium (MRLC) (<https://www.mrlc.gov/>). At the time of writing, the most current NLCD products for land cover and impervious surface are in the year 2011, while the NLCD 2016 products are still in production. Assisted by Landsat 5 Thematic Mapper (TM) imagery, NLCD land cover product provides sixteen unique classes with a resolution of 30m, in which three classes

indicate potential high population concentration: 1) Developed – Low Intensity; 2) Developed – Medium Intensity and 3) Developed – High Intensity [31]. Only the aforementioned three classes were extracted and further resampled to 100m under a majority sampling rule. The NLCD 2011 impervious surface product provides the percent developed imperviousness with a resolution of 30m [32]. It was also resampled to 100m to match the population grid size via a bilinear sampling rule. The nighttime light, land cover and impervious surface serve as three different weighting layers in contrast with the weighting layers derived from Microsoft building footprints.

4 METHODOLOGY

4.1 Dasymetric Mapping

Dasymetric mapping is the technique that employs a series of spatial partitions to introduce a higher resolution level into a dataset than the level at which the data were originally captured [33]. Geospatial layers with finer resolution than the base mapping unit are used to disaggregate the population data, consequently deriving a finer population dataset. Given the known population at source zone t (P_t), the disaggregating process follows:

$$P_i^e = P_t \times \frac{A_i \times W_i}{\sum_i A_i \times W_i} \quad (i \in R^t) \quad (1)$$

where P_i^e refers to the estimated population in the target zone i . The source zone represents a discrete geographic unit where population statistics are reported, i.e., the census tract. The target zones represent finer zones within each source zone, i.e., 100m cells within census tract t . A_i and W_i respectively denote the size of the cell and the corresponding weight related to the population distribution in the cell. Note that the disaggregating process assigns the population into 100m cells based on the weighting layer while preserves the sum of the population originally reported at each census tract, i.e. $P_t = \sum_{i \in R^t} P_i^e$.

4.2 Weighting Scenarios

Several weighting scenarios were designed to explore the potential of building footprints in population disaggregation in the CONUS. Those weighting scenarios differ in the design of weight in each targeted cell i (W_i in Equation 1). Positive relationships were assumed between the estimated population and 1) building footprint size (original: BF_s , trimmed: BF'_s) 2) building footprint count (original: BF_c , trimmed: BF'_c); 3) building footprint size* count (original: BF_{sc} , trimmed: BF'_{sc}); 4) observed light intensity (NTL) and 5) impervious surface percentage (ISP). Note that the population disaggregation was conducted separately using original building footprints and using building footprints trimmed by crowdsourced OSM land use data. Additionally, two other scenarios were added by assuming the population is uniformly distributed 1) in all cells across the census tract (UNIF) and 2) in habitable cells where cells were labeled as “developed” as land use type across the census tract (LC).

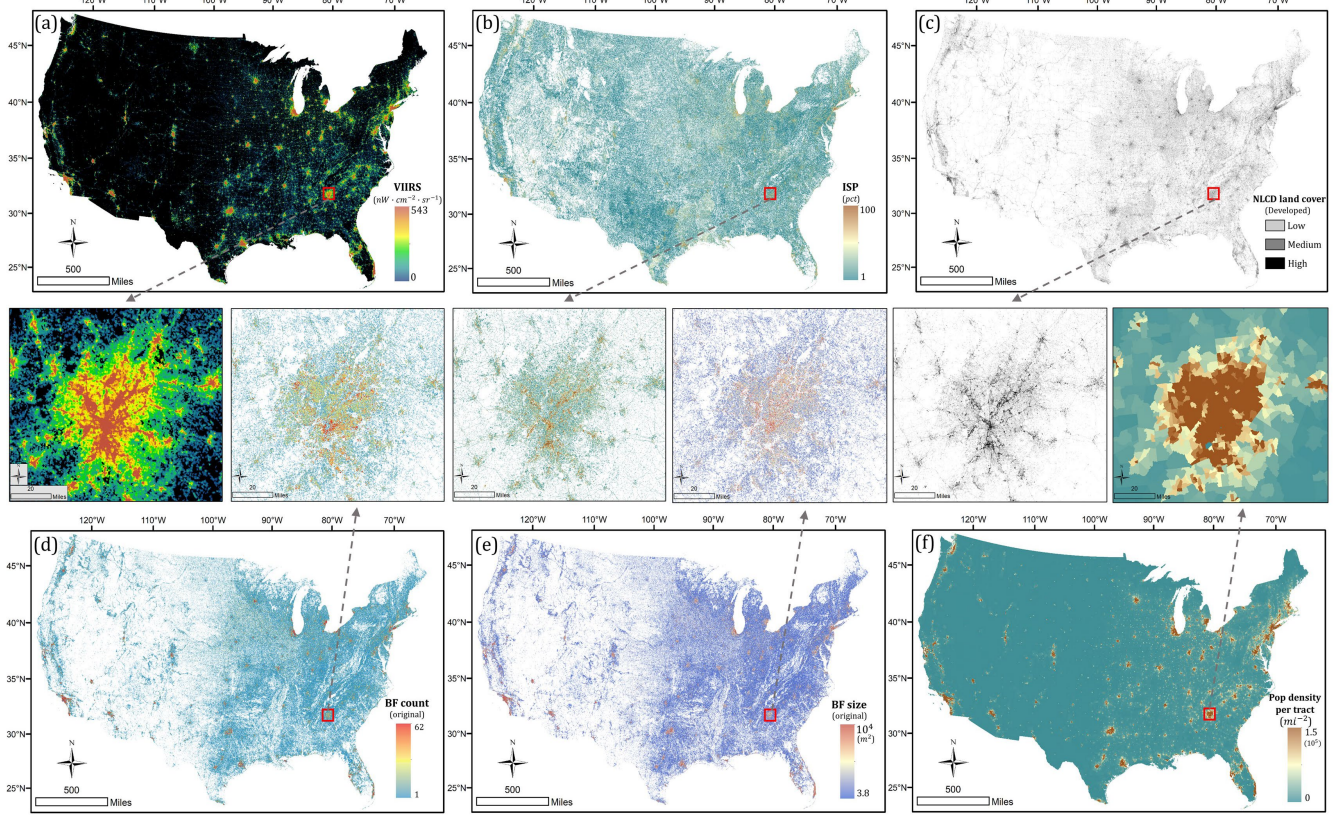


Figure 1: Selected weighting scenarios. (a) NTL; (b) ISP; (c) LC; (d) BF_c ; (e) BF_s ; (f) UNIF

Weighting scenarios in detail can be found in Table A in the Appendix. Figure 1 shows six selected weighting layers: NTL (a), ISP (b), LC (c), BF_c (d), BF_s (e) and UNIF (f), at CONUS-scale. Notable similarity can be observed among weighting layers of BF_c , BF_s and ISP, given their continuous values and identical resolution (after resampling). In comparison, the weighting layer of LC is categorical since the habitable regions defined in this study only comprise developed land cover types of “low”, “medium”, and “high” (Figure 1c).

4.3 Metrics of Assessment

To evaluate the performances of weighting scenarios, six basic quantitative measurements of accuracy were used in this study. Those measurements include: 1) Root Mean Square Error (RMSE); 2) Mean Absolute Error (MAE); 3) Overall Relative Error (ORE); 4) Coefficient of Efficiency (CoE); 5) Systematic Error (SE) and 6) Modified Index of Agreement (MIoA). Those quantitative measurements were used to measure the discrepancy between the true block group population and the estimated block group population. Their calculations are respectively described in Equations 2-7:

$$RMSE = \sqrt{\frac{\sum_{j=1}^n (P_j^e - P_j^g)^2}{n}} \quad (2)$$

$$MAE = \frac{\sum_{j=1}^n |P_j^e - P_j^g|}{n} \quad (3)$$

$$ORE = \frac{\sum_{j=1}^n \left| \frac{P_j^e - P_j^g}{P_j^g} \right|}{n} \times 100\% \quad (4)$$

$$CoE = 1 - \frac{\sum_{j=1}^n (P_j^g - P_j^e)^2}{\sum_{j=1}^n (P_j^g - \bar{P}_j^g)^2} \quad (5)$$

$$SE = \frac{\sum_{j=1}^n P_j^e - P_j^g}{n} \quad (6)$$

$$MIoA = 1 - \frac{\sum_{j=1}^n |P_j^g - P_j^e|}{\sum_{j=1}^n (|P_j^e - \bar{P}_j^g| + |P_j^g - \bar{P}_j^g|)} \quad (7)$$

where P_j^e and P_j^g respectively denote the estimated population and true population in block group j . \bar{P}_j^g denotes the mean true population in all block groups. P_t , P_j^e and P_i^e satisfy 1) $P_t = \sum_{j \in R^t} P_j^e$ and 2) $P_j = \sum_{i \in R^j} P_i^e$.

5 RESULTS

The performance of weighting scenarios was tested after they were applied to derive the population grid from census tracts. Those weighting scenarios include: BF_s , BF_c , BF_{sc} , BF'_s , BF'_c , BF'_{sc} , NTL, LC, ISP, and UNIF (details in Table A). The derived population grid was then reaggregated to block group level for evaluation. Figure 2 presents the scatter plot histogram for all 266,330 block groups within the CONUS. In general, population grid disaggregated using building footprint statistics tends to have a higher coefficient of determination (R^2) compared to other commonly used weighting layers, including NTL (Figure 2g), LC (Figure 2h), and ISP (Figure 2i), indicating that building footprint statistics introduced less uncertainty and are more relevant to population distribution at the block group level. Notable uncertainty was observed when population distribution was assumed uniform within each census tract (Figure 2j). The poor performance of the UNIF scenario proved the ubiquitous existence of heterogeneity within a rather small geographic unit like the census tract. BF'_s (building size after trimming) as weighting scenario was found to have the highest R^2 ($R^2 = 0.794$) among all scenarios while UNIF the lowest ($R^2 = 0.344$).

In addition, metrics of accuracy assessment, including RMSE, MAE, ORE, SE, CoE, and MIoA for all weighting scenarios, are presented in Table 1. Distinct advantage can be found when

comparing the population disaggregation method using building footprint statistics (in both original and trimmed cases) with that using NTL, LC, ISP, and UNIF. Building footprint statistics greatly outperformed other weighting scenarios, specifically in ORE and CoE. OREs for building footprints, for example, are all lower than 30% while OREs for other scenarios all above 30%. With a range from minus infinity to 1, CoE statistic indicated a better agreement of estimated population and ground-truth population when building footprints were applied since CoEs for building footprints all reach above 0.7, a rather high model agreement. UNIF was found the worst compared with other scenarios, especially in the CoE statistic. The CoE of -0.318 for the UNIF scenario confirmed again that uniform distribution should not be assumed at the census tract level. Moreover, the improvement of metrics like RMSE, MAR, and MIoA when building footprints were applied in the population disaggregation process indicated a stronger relationship between building footprints and population distribution. Among all scenarios, BF'_s achieved best performances in all assessment metrics except SE. Building size transcends building count, presumably due to its consideration of two-dimension building holding capacity. Despite the lack of vertical dimension, building size was still proved superior to building count, especially after the trimming process in which a large amount of non-residential buildings were removed.

Table 1: Accuracy assessment for all weighting scenarios

Scenarios	RMSE	MAE	ORE	SE	CoE	MIoA
Building Footprints (original)						
BF_c						
BF_c	464.29	311.34	26.36%	0.175	0.766	0.751
BF_s	462.40	316.27	27.74%	1.265	0.769	0.748
BF_{sc}	464.46	312.97	26.24%	1.297	0.767	0.752
Building Footprints (trimmed)						
BF'_c						
BF'_c	480.96	313.53	26.24%	3.517	0.751	0.751
BF'_s	444.43	298.74	25.55%	3.505	0.787	0.762
BF'_{sc}	490.06	320.38	26.44%	3.536	0.741	0.749
NTL	723.58	500.25	42.89%	0.529	0.432	0.635
LC	617.99	429.12	38.85%	4.075	0.586	0.672
ISP	643.68	447.95	40.48%	4.475	0.551	0.661
UNIF	1102.57	606.75	52.08%	37.955	-0.318	0.578

Note. The best performance for each individual assessment metric is highlighted in bold

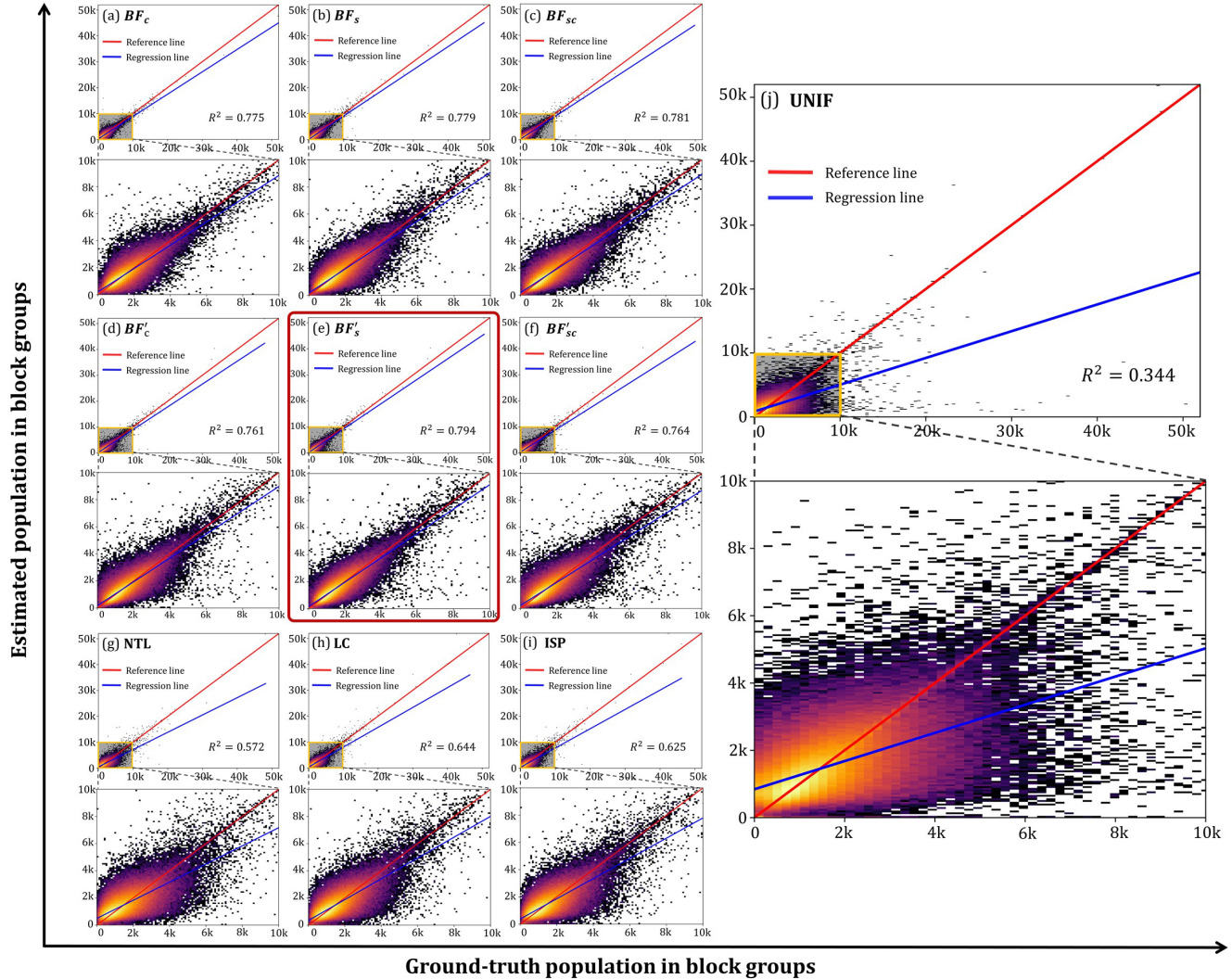


Figure 2: Performances of designed weighting scenarios in CONUS evaluated at block group level. (a) Original building count; (b) original building size; (c) original building size*count; (d) trimmed building count; (e) trimmed building size; (f) trimmed building size*count; (g) nighttime light intensity; (h) land cover; (i) impervious surface percentage; (j) uniform distribution in census tracts.

Population disaggregation for the entire CONUS was further conducted using BF'_s , the scenario with the best performance. Figure 3 presents the difference between the population disaggregation using BF'_s (trimmed) and BF_s (original) in an example site in Addison, TX. From downloaded OSM data, there are a total of seven land use types in this site, including “Retail”, “Recreation”, “Park”, “Industrial”, “Grass”, “Forest” and “Commercial”. As the selected site is within downtown Addison, land use of “Commercial” is dominant (Figure 3b). Due to the fact that all of these land use types above are unlikely to include residential buildings, original building footprints (Figure 3a) were removed if they were contained by those land use polygons,

resulting in the trimmed building footprints (Figure 3c). Population grids were further derived via a dasymetric mapping method (Section 4.1) using building size as a weighting scenario for original building footprints (Figure 3d) and trimmed building footprints (Figure 3e). The results suggested that the population grid using original building footprints falls short as it assigns a large amount of population to the three major commercial zones (within black dashed lines). In comparison, the population grid using trimmed building footprints is more reasonable thanks to the trimming process that greatly contributes to the removal of buildings that are unlikely to be residential within this selected urban fabric.

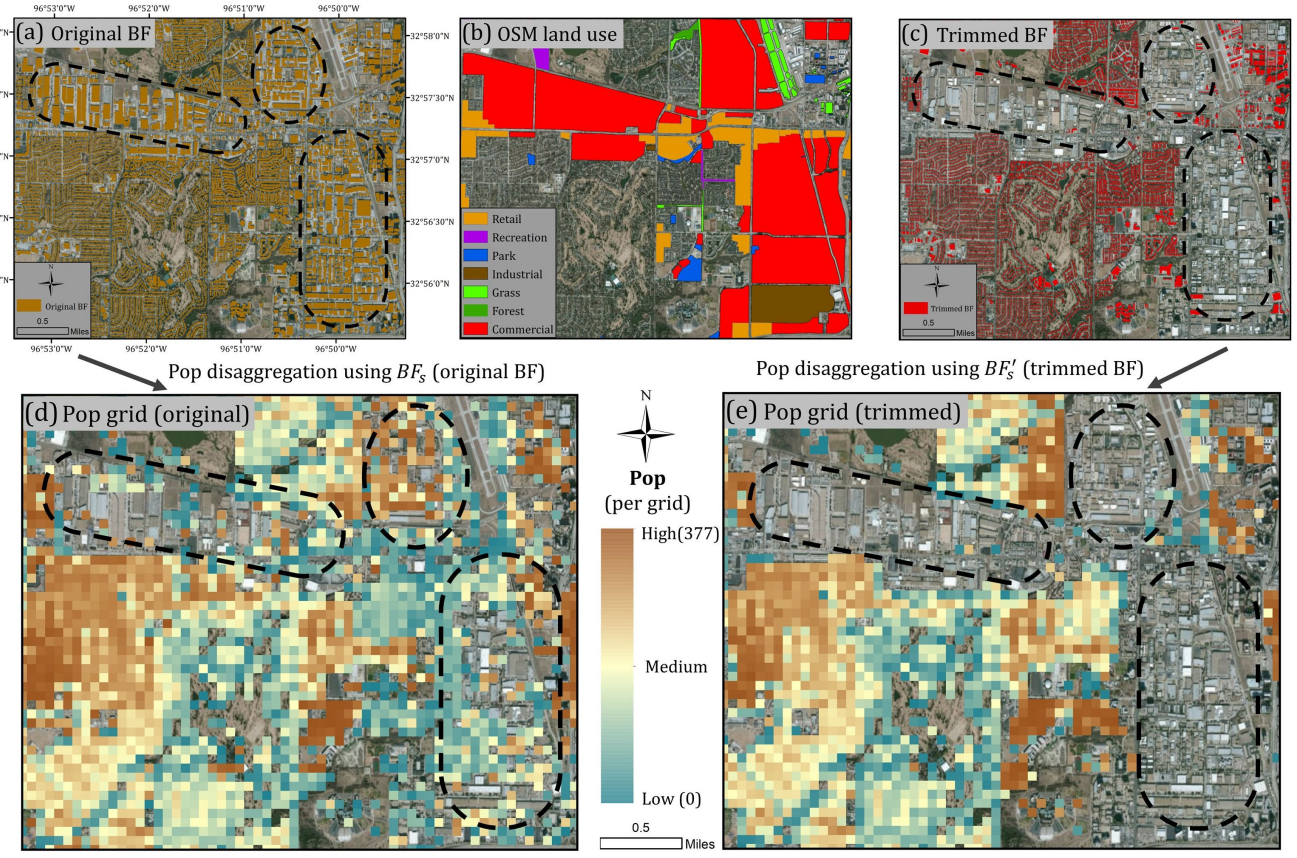


Figure 3. Example of population grid in Addison, TX before and after the trimming process. (a) Original building footprints; (b) Crowdsourced land use types derived from OSM; (c) Trimmed building footprints after removing building footprints within non-residential land use polygons; (d) Population grid using original building footprint size; (e) Population grid using trimmed building footprint size.

6 LIMITATIONS AND DIRECTIONS

Although this study has merits, some limitations need to be mentioned. The Microsoft building footprint dataset used in this study does not contain any building height information. The lack of vertical dimension in buildings potential introduces great uncertainty in estimating the overall building holding capacity, leading to the underestimation of the population of highly urbanized areas with high-rise buildings. Even though the OSM data successfully removed a majority of high-rise commercial use buildings in urban areas, the existence of high-rise mixed-use and high-rise residential buildings poses a great challenge in population disaggregation. Future work should focus on incorporating the vertical dimension of buildings, potentially derived from LiDAR [34] or using photogrammetric approaches [35].

Secondly, as the Bing Imagery is a composite of multiple imaging sources in various temporal periods, it is difficult to know the exact date for individual pieces of data [36]. The temporal ambiguity of the Microsoft building dataset might cause problems

for studies that require certain temporal restrictions. Further study should focus on updating those building footprints to generate population grids with temporal continuation. The emergence of commercialized high-resolution images coupled with well-trained deep learning models creates a great opportunity for the automatic extraction of buildings at large-scale.

Thirdly, this study compared building footprints as weighting layers with other commonly used layers. However, the resolution of the layers in comparison varies. In addition, the evaluation was only performed on the level of block groups due to the lack of finer ground-truth data. Further comparisons on other finer weight layers and finer ground-truth population distribution are needed.

Finally, the voluntary participation of OSM raises other concerns. The spatial bias of OSM has been noted as the completeness of OSM generally favors urban areas rather than rural areas. Besides, the quality of the OSM land use dataset tends to vary greatly in different regions [37]. Those uncertainties might cause notable spatial biases in the resulted population grids. In light of the limitations above, a better strategy for categorizing building usage at the CONUS-scale is in great need.

7 CONCLUSION

This study explores the potential of buildings as a proxy in generating high-resolution (100m) population grids in the entire CONUS. A total of 125 million computer-generated building footprints in the CONUS, further trimmed by OSM land use polygons, were used to disaggregate census tract population from the latest ACS 5-year estimates (2013-2017). Derived population grids were then reaggregated at block group level to compare with the ground-truth block group population from the ACS estimates. The effectiveness of building footprints was further evaluated against other commonly used weighting layers. The results suggest that weighting layers from building footprints greatly outperform other layers, including the uniform layer, the light intensity layer, the land cover layer, and the impervious surface layer. Among all the layers, building footprint size after trimming (BF'_S) achieved the best performance, presumably due to its consideration of two-dimensional building holding capacity. Despite the limitations of the current Microsoft building footprint dataset, it is a valuable source for creating high-resolution population grids that consider the great heterogeneity of population distribution at micro-level. Future works should focus on incorporating the vertical dimension of buildings, designing a better building categorization strategy, and updating those building footprints to generate population grid products with temporal continuation.

REFERENCES

- [1] Nadim, F., Kjekstad, O., Peduzzi, P., Herold, C., & Jaedicke, C. (2006). Global landslide and avalanche hotspots. *Landslides*, 3(2), 159-173.
- [2] Ahola, T., Virrantaus, K., Krisp, J. M., & Hunter, G. J. (2007). A spatio-temporal population model to support risk assessment and damage analysis for decision-making. *International Journal of Geographical Information Science*, 21(8), 935-953.
- [3] Linard, C., Alegana, V. A., Noor, A. M., Snow, R. W., & Tatem, A. J. (2010). A high resolution spatial population database of Somalia for disease risk mapping. *International Journal of Health Geographics*, 9(1), 45.
- [4] Smith, S. K., Nogle, J., & Cody, S. (2002). A regression approach to estimating the average number of persons per household. *Demography*, 39(4), 697-712.
- [5] Steinnocher, K., Köstl, M., & Weichselbaum, J. (2011, February). Grid-based population and land take trend indicators—new approaches introduced by the geoland2 core Information Service for Spatial Planning. In *NTTS conference, Brussels*.
- [6] Tatem, A. J. (2017). WorldPop, open data for spatial demography. *Scientific data*, 4.
- [7] Li, X., & Zhou, W. (2018). Dasymetric mapping of urban population in China based on radiance corrected DMSP-OLS nighttime light and land cover data. *Science of the total environment*, 643, 1248-1256.
- [8] Wardrop, N. A., Jochem, W. C., Bird, T. J., Chamberlain, H. R., Clarke, D., Kerr, D., ... & Tatem, A. J. (2018). Spatially disaggregated population estimates in the absence of national population and housing census data. *Proceedings of the National Academy of Sciences*, 115(14), 3529-3537.
- [9] Wang, L., Wang, S., Zhou, Y., Liu, W., Hou, Y., Zhu, J., & Wang, F. (2018). Mapping population density in China between 1990 and 2010 using remote sensing. *Remote sensing of environment*, 210, 269-281.
- [10] Lloyd, C. D., Catney, G., Williamson, P., & Bearman, N. (2017). Exploring the utility of grids for analysing long term population change. *Computers, Environment and Urban Systems*, 66, 1-12.
- [11] Klein Goldewijk, K., Beusen, A., & Janssen, P. (2010). Long-term dynamic modeling of global population and built-up area in a spatially explicit way: HYDE 3.1. *The Holocene*, 20(4), 565-573.
- [12] Klein Goldewijk, K., Beusen, A., Van Drecht, G., & De Vos, M. (2011). The HYDE 3.1 spatially explicit database of human-induced global land-use change over the past 12,000 years. *Global Ecology and Biogeography*, 20(1), 73-86.
- [13] Doxsey-Whitfield, E., MacManus, K., Adamo, S. B., Pistolesi, L., Squires, J., Borkovska, O., & Baptista, S. R. (2015). Taking advantage of the improved availability of census data: a first look at the gridded population of the world, version 4. *Papers in Applied Geography*, 1(3), 226-234.
- [14] Balk, D., Pozzi, F., Yetman, G., Deichmann, U., & Nelson, A. (2005, March). The distribution of people and the dimension of place: methodologies to improve the global estimation of urban extents. In International Society for Photogrammetry and Remote Sensing, proceedings of the urban remote sensing conference (pp. 14-16).
- [15] Freire, S., & Pesaresi, M. (2015). GHS population grid, derived from GPW4, multitemporal (1975, 1990, 2000, 2015). European Commission, Joint Research Centre (JRC). PID: http://data.europa.eu/89h/jrcgshs-ghs_pop_gpw4_globe_r2015a.
- [16] Dobson, J. E., Bright, E. A., Coleman, P. R., Durfee, R. C., & Worley, B. A. (2000). LandScan: a global population database for estimating populations at risk. *Photogrammetric engineering and remote sensing*, 66(7), 849-857.
- [17] Frye, C., Wright, D. J., Nordstrand, E., Terborgh, C., & Foust, J. (2018). Using Classified and Unclassified Land Cover Data to Estimate the Footprint of Human Settlement. *Data Science Journal*, 17.
- [18] Sorichetta, A., Hornby, G. M., Stevens, F. R., Gaughan, A. E., Linard, C., & Tatem, A. J. (2015). High-resolution gridded population datasets for Latin America and the Caribbean in 2010, 2015, and 2020. *Scientific data*, 2, 150045.
- [19] Azar, D., Engstrom, R., Graesser, J., & Comenetz, J. (2013). Generation of fine-scale population layers using multi-resolution satellite imagery and geospatial data. *Remote Sensing of Environment*, 130, 219-232.
- [20] Tiecke, T. G., Liu, X., Zhang, A., Gros, A., Li, N., Yetman, G., ... & Dang, H. A. H. (2017). Mapping the world population one building at a time. *arXiv preprint arXiv:1712.05839*.
- [21] Yuan, J. (2018). Learning building extraction in aerial scenes with convolutional networks. *IEEE transactions on pattern analysis and machine intelligence*, 40(11), 2793-2798.
- [22] Huang, Z., Cheng, G., Wang, H., Li, H., Shi, L., & Pan, C. (2016, July). Building extraction from multi-source remote sensing images via deep deconvolution neural networks. In *2016 IEEE International Geoscience and Remote Sensing Symposium (IGARSS)* (pp. 1835-1838). IEEE.
- [23] Murdock, A.P., Harfoot, A.J.P., Martin, D., Cockings, S. and Hill, C. (2015). OpenPopGrid: an open gridded population dataset for England and Wales. GeoData, University of Southampton, <http://openpopgrid.geodata.soton.ac.uk/>
- [24] Microsoft USBuildingFootprints. (2018). Retrieved from <https://github.com/Microsoft/USBuildingFootprints>
- [25] Ramm, F., Names, I., Files, S. S., Catalogue, F., Features, P., Features, N., & Cars, C. (2014). OpenStreetMap Data in Layered GIS Format. *Version 0.6.7*.
- [26] Chen, X., & Nordhaus, W. (2015). A test of the new VIIRS lights data set: Population and economic output in Africa. *Remote Sensing*, 7(4), 4937-4947.
- [27] Patel, N. N., Anguili, E., Gamba, P., Gaughan, A., Lisini, G., Stevens, F. R., ... & Trianni, G. (2015). Multitemporal settlement and population mapping from Landsat using Google Earth Engine. *International Journal of Applied Earth Observation and Geoinformation*, 35, 199-208.
- [28] Elvidge, C. D., Baugh, K., Zhizhin, M., Hsu, F. C., & Ghosh, T. (2017). VIIRS night-time lights. *International Journal of Remote Sensing*, 38(21), 5860-5879.
- [29] Mills, S., Weiss, S., & Liang, C. (2013, September). VIIRS day/night band (DNB) stray light characterization and correction. In *Earth Observing Systems XVIII* (Vol. 8866, p. 88661P). International Society for Optics and Photonics.
- [30] Holt, J. B., Lo, C. P., & Hodler, T. W. (2004). Dasymetric estimation of population density and areal interpolation of census data. *Cartography and Geographic Information Science*, 31(2), 103-121.
- [31] Homer, C., Dewitz, J., Yang, L., Jin, S., Danielson, P., Xian, G., ... & Megown, K. (2015). Completion of the 2011 National Land Cover Database for the conterminous United States—representing a decade of land cover change information. *Photogrammetric Engineering & Remote Sensing*, 81(5), 345-354.
- [32] Xian, G. Z., Homer, C. G., Dewitz, J., Fry, J., Hossain, N., & Wickham, J. (2011). Change of impervious surface area between 2001 and 2006 in the conterminous United States. *Photogrammetric Engineering and Remote Sensing*, 77(8), 758-762.
- [33] Azar, D., Engstrom, R., Graesser, J., & Comenetz, J. (2013). Generation of fine-scale population layers using multi-resolution satellite imagery and geospatial data. *Remote Sensing of Environment*, 130, 219-232.
- [34] Rottensteiner, F., & Briese, C. (2002, September). A new method for building extraction in urban areas from high-resolution LIDAR data. In *International Archives of Photogrammetry Remote Sensing and Spatial Information Sciences* (Vol. 34, No. 3/A, pp. 295-301). NATURAL RESOURCES CANADA.
- [35] Stal, C., Tack, F., De Maeyer, P., De Wulf, A., & Goossens, R. (2013). Airborne photogrammetry and lidar for DSM extraction and 3D change detection over an urban area—a comparative study. *International Journal of Remote Sensing*, 34(4), 1087-1110.
- [36] Microsoft. (2019, March 04). Microsoft/USBuildingFootprints. Retrieved from <https://github.com/Microsoft/USBuildingFootprints>
- [37] Quattrone, G., Capra, L., & De Meo, P. (2015, February). There's no such thing as the perfect map: Quantifying bias in spatial crowd-sourcing datasets. In *Proceedings of the 18th ACM Conference on Computer Supported Cooperative Work & Social Computing* (pp. 1021-1032). ACM.

Appendix

Table A: Weighting scenarios in detail

Scenario names and annotations	Weighting method	Description
Building footprint (original)		Population is assumed to be distributed proportionally to 1) total building size; 2) total building count; and 3) size*count within cell i . The building footprints are the original product without trimming.
Size (BF_s) Count (BF_c) Size*Count (BF_{sc})	$W_i = \begin{cases} \sum bf_s \\ \sum bf_c, \text{ where } bf \text{ is within cell } i \\ \sum bf_{sc} \end{cases}$	
Building footprint (trimmed)		Trimmed building footprint (bf') denotes the building footprint that is not within uninhabitable areas. Those uninhabitable areas are within OSM polygons tagged as commercial, forest, grass, park, recreation ground, vineyard, industrial, meadow, military, natural reserve, orchard, quarry, scrub, and cemetery. In addition, building footprints with size less than $50 m^2$ and more than $5000 m^2$ were removed as they are not likely to be residential.
Size (BF'_s) Count (BF'_c) Size*Count (BF'_{sc})	$W_i = \begin{cases} \sum bf'_s \\ \sum bf'_c, \text{ where } bf' \text{ is within cell } i \\ \sum bf'_{sc} \end{cases}$	
Nighttime light intensity (NTL)	$W_i = NTL_i$	Population is assumed to be distributed proportionally to light intensity within each census tract. Thus, the population for each cell i is weighted by its observed light intensity.
Land cover (LC)	$W_i = \frac{A_i}{\sum_i A_i}$, where A_i is within “developed” as LC type, including low density, medium density, and high density	Population is assumed to be uniformly distributed within habitable cells in each census tract. Those habitable cells denote land cover type as “developed”, including low density, medium density, and high density.
Impervious surface percentage (ISP)	$W_i = ISP_i$	Population is assumed to be distributed proportionally to ISP within each census tract. Thus, the population for each cell i is weighted by its ISP.
Uniform (UNIF)	$W_i = \frac{A_i}{\sum_i A_i}$	Population is assumed to be uniformly distributed across each census tract. Therefore, population assigned to each cell is proportional to its percentage of coverage in each census tract.

Note. Cell i is within census tract t , i.e., $i \in R^t$.